



## University of Dundee

### ELIGULUM-A regulates lateral branch and leaf development in barley

Okagaki, Ron J.; Haaning, Allison; Bilgic, Hatice; Heinen, Shane; Druka, Arnis; Bayer, Micha; Waugh, Robbie; Muehlbauer, Gary J.

*Published in:*  
Plant Physiology

*DOI:*  
[10.1104/pp.17.01459](https://doi.org/10.1104/pp.17.01459)

*Publication date:*  
2018

*Document Version*  
Peer reviewed version

[Link to publication in Discovery Research Portal](#)

#### *Citation for published version (APA):*

Okagaki, R. J., Haaning, A., Bilgic, H., Heinen, S., Druka, A., Bayer, M., ... Muehlbauer, G. J. (2018). ELIGULUM-A regulates lateral branch and leaf development in barley. *Plant Physiology*. DOI: 10.1104/pp.17.01459

#### **General rights**

Copyright and moral rights for the publications made accessible in Discovery Research Portal are retained by the authors and/or other copyright owners and it is a condition of accessing publications that users recognise and abide by the legal requirements associated with these rights.

- Users may download and print one copy of any publication from Discovery Research Portal for the purpose of private study or research.
- You may not further distribute the material or use it for any profit-making activity or commercial gain.
- You may freely distribute the URL identifying the publication in the public portal.

#### **Take down policy**

If you believe that this document breaches copyright please contact us providing details, and we will remove access to the work immediately and investigate your claim.

1 **Short Title**

2 Regulation of Leaf and Lateral Branch Development

3

4

5 Gary J. Muehlbauer

6

7

8 Department of Agronomy and Plant Genetics, and Department of Plant and Microbial Biology,  
9 University of Minnesota, St. Paul, MN 55108

10

11

12

13 *ELIGULUM-A* regulates lateral branch and leaf development in barley

14

15 Ron J. Okagaki<sup>1</sup>, Allison Haaning<sup>1</sup>, Hatice Bilgic<sup>1</sup>, Shane Heinen<sup>1</sup>, Arnis Druka<sup>2</sup>, Micha Bayer<sup>2</sup>,  
16 Robbie Waugh<sup>2</sup> and Gary J. Muehlbauer<sup>1,3</sup>

17 <sup>1</sup>Department of Agronomy and Plant Genetics, University of Minnesota, St. Paul, MN 55108

18 <sup>2</sup>The James Hutton Institute, Dundee, United Kingdom

19 <sup>3</sup>Department of Plant and Microbial Biology, University of Minnesota, St. Paul, MN 55108

20

21 One-sentence summary: The barley *ELIGULUM-A* gene regulates lateral branch development  
22 and acts to establish the blade–sheath boundary during leaf development.

23

24 Author contributions

25 R.J.O. performed most of the experiments and wrote the manuscript; A.H. performed the RNA *in*  
26 *situ* hybridizations and edited the manuscript; H.B.L. developed genetic materials; S.H.  
27 conducted the suppressor screen; A.D. performed the bioinformatics analysis; M.B. performed  
28 the bioinformatics analysis; R.W. oversaw the bioinformatics analysis and edited the manuscript;  
29 G.J.M. conceived the original research plan and edited the manuscript.

30

31 Funding information

32 Department of Agriculture-CSREES-NRI Plant Growth and Development program grant # 2004-  
33 03440, and funds received from the Triticeae Coordinated Agricultural Project, US Department  
34 of Agriculture/National Institute for Food and Agriculture grant number 2011-68002-30029 to  
35 G.J.M.

36

37

38 Corresponding author

39 G.J.M. muehl003@umn.edu

40 **ABSTRACT**

41 The shoot apical and axillary meristems control shoot development, effectively influencing lateral branch  
42 and leaf formation. The barley (*Hordeum vulgare* L.) *uniculm2* (*cul2*) mutation blocks axillary meristem  
43 development and mutant plants lack lateral branches (tillers) that normally develop from the crown. A  
44 genetic screen for *cul2* suppressors recovered two recessive alleles of *ELIGULUM-A* (*ELI-A*) that  
45 partially rescued the *cul2* tillering phenotype. Mutations in *ELI-A* produce shorter plants with fewer tillers  
46 and disrupt the leaf blade–sheath boundary, producing liguleless leaves and reduced secondary cell wall  
47 development in stems and leaves. *ELI-A* is predicted to encode an un-annotated protein containing a  
48 RNaseH-like domain that is conserved in land plants. *ELI-A* transcripts accumulate at the preligule  
49 boundary, the developing ligule, leaf margins, cells destined to develop secondary cell walls, and cells  
50 surrounding leaf vascular bundles. Recent studies have identified regulatory similarities between  
51 boundary development in leaves and lateral organs. Interestingly, we observed *ELI-A* transcripts at the  
52 preligule boundary, suggesting that *ELI-A* contributes to boundary formation between the blade and  
53 sheath. However, we did not observe *ELI-A* transcripts at the axillary meristem boundary in leaf axils,  
54 suggesting that *ELI-A* is not involved in boundary development for axillary meristem development. Our  
55 results show that *ELI-A* contributes to leaf and lateral branch development by acting as a boundary gene  
56 during ligule development but not during lateral branch development.

57

## 58 INTRODUCTION

59 Leaves and tillers, the vegetative branches that form at the base of grass plants, are key  
60 determinants of grass shoot architecture. Tillers develop from axillary meristems and undergo  
61 three distinct morphological stages: (1) initiation of an axillary meristem in the leaf axil; (2)  
62 development of leaf primordia on the axillary meristem to form an axillary bud; and (3)  
63 elongation of internodes into a tiller with the potential to form a grain-bearing spike (Schmitz  
64 and Theres, 2005). Primary tillers form in leaf axils on the main stem, and secondary and higher  
65 order tillers form in axils of leaves on primary tillers and subsequent tillers, respectively. Grass  
66 leaves develop from the flanks of the shoot apical meristem and axillary meristems, and are  
67 composed of a proximal sheath and distal blade divided by the ligular boundary. The ligular  
68 region is composed of the ligule, an outgrowth of an epidermal tissue flap, and the auricle.  
69 Auricles have two parts, a band of small cells separating the sheath from the blade and a flap of  
70 tissue growing out from the leaf margin that wraps around the stem in some species (Sylvester et  
71 al., 1990; Becraft et al., 1990). Both tillers and leaves are important agricultural traits for cereal  
72 crops and have been extensively studied (reviewed in Wang and Li, 2008; Lewis and Hake,  
73 2015; Mathan et al., 2016). However, our understanding of the inter-relatedness of their genetic  
74 control is early in its fruition.

75 Positional information is important for morphogenesis and boundaries between cell types  
76 are often the location of new tissue development. Thus, the role of boundary formation in  
77 axillary meristem development is an intense area of study (reviewed in: Žádníková and Simon,  
78 2014; Hepworth and Pautot, 2015; Wang et al., 2016). The *Arabidopsis thaliana* *REGULATORS*  
79 *OF AXILLARY MERISTEMS1* (*RAX1*) and *CUP-SHAPED COTYLEDON2* (*CUC2*) genes were  
80 identified by their expression pattern and reduced-branching mutant phenotypes, and were found  
81 to establish the boundary for axillary meristem development (Keller et al., 2006; Müller et al.,  
82 2006). Other boundary genes show the expected expression pattern but lack a clear axillary  
83 meristem phenotype in mutant plants. Plants over expressing *Arabidopsis* *BLADE-ON-PETIOLE*  
84 (*BOP*) show a branching phenotype, producing extra paraclades in leaf nodes (Ha et al., 2007).  
85 The role of *Arabidopsis* *LATERAL ORGAN FUSION* (*LOF1*) in axillary meristem development  
86 was revealed by double mutants with its homolog, *LOF2* (Lee et al., 2009). The *Arabidopsis*  
87 *REGULATOR OF AXILLARY MERISTEM FORMATION1* (*ROX1*) has a subtle phenotype but is  
88 involved in axillary meristem development (Yang et al., 2012). However, the role of *ROX1* in

89 axillary meristem development is more obvious in other species such as rice and maize,  
90 highlighting the importance of comparative work to fully delineate developmental pathways  
91 (Komatsu et al. 2003; Gallavotti et al. 2004). These studies, and others, have identified genes  
92 acting in axillary meristem boundary formation and it appears a number of these genes help  
93 establish other developmental boundaries.

94 Boundary formation is also critical for leaf patterning (reviewed in Bar and Ori, 2014;  
95 Lewis and Hake, 2015). Tomato plants produce compound leaves with several pairs of lateral  
96 leaflets and a terminal leaflet, with each leaflet having multiple lobes. *Goblet* (*Gob*) is one gene  
97 controlling this process, and *Gob* encodes a homolog of *CUC1/2* (Berger et al., 2009). *Gob*  
98 mutations also repress axillary meristem development (Busch et al., 2011). *Potato leaf* (*C*) and  
99 *blind* are recent duplications of the tomato *RAX1* homolog and sub-functionalization of these  
100 duplicated genes gave *blind* a role in axillary meristem development and *C* a role in leaf  
101 development (Busch et al., 2011). In *Arabidopsis*, *CUC2* functions similarly to produce serrated  
102 leaves (Nikovics et al., 2006; Bilsborough et al., 2010). It is now evident that many of the same  
103 genes act to establish boundaries for meristem and leaf development (Hepworth and Pautot,  
104 2015; Wang et al., 2016)

105 The identification of genes with dual roles in boundary demarcation and leaf and axillary  
106 meristem development prompted Busch and colleagues (2011) to propose a conserved genetic  
107 system that establishes axillary meristems and determines leaf shape. A related genetic system  
108 for maize leaf and lateral organ initiation was recently proposed as well (Johnston et al., 2014).  
109 Transcriptome analysis of laser-dissected tissues from the maize preligule region identified genes  
110 expressed at the blade–sheath boundary that are homologs of previously identified genes  
111 involved in lateral organ initiation (Johnston et al., 2014). Among the differentially expressed  
112 genes were the maize *CUC2* and *BOP* homologs. RNA *in situ* hybridization experiments  
113 showed maize *CUC2-like* transcripts accumulating in the preligule band, the cleft of developing  
114 ligules, and at the location of lateral branch initiation. The maize *BOP-like* transcripts  
115 accumulated in developing ligules, leaf axils and axillary meristems (Johnston et al., 2014). The  
116 barley *UNICULME4* (*CULA*) gene is the barley *BOP* homolog (Tavakol et al., 2015), and plants  
117 carrying mutations in *CULA* are defective in both axillary meristem and ligule development. In  
118 addition, *CULA* is expressed in developing ligules, leaf axils and axillary meristems, and defines

119 the boundaries of ligule and axillary bud development like the maize *BOP* homolog (Tavakol et  
120 al., 2015).

121 In this study, we conducted a genetic suppressor screen using a mutant that does not  
122 make tillers, *uniculm2* (*cul2*) (Babb and Muehlbauer, 2003), and identified two mutations in the  
123 *ELIGULUM-A* (*ELI-A*) gene that promoted axillary meristem development and tillering in the  
124 *cul2* mutant background. Mutations in *ELI-A* have been previously described as pleiotropic with  
125 altered ligule development, reduced plant height, weak culms, and compact spikes (Lundqvist  
126 and Franckowiak, 2002). Additional characterization showed that *eli-a* mutant plants exhibited  
127 reduced tillering and secondary cell wall formation compared with the non-mutant backcross  
128 parent line. We isolated the *ELI-A* gene and determined that it encodes a previously un-annotated  
129 protein. RNA *in situ* hybridizations showed that *ELI-A* transcripts are found in the preligular  
130 region, the developing ligule, leaf margins, cells destined to develop secondary cell walls, and in  
131 cells surrounding leaf vascular bundles. Taken together, these observations show that *ELI-A* plays  
132 a role in ligule and axillary meristem development. We propose that *ELI-A* functions in  
133 establishing a boundary during ligule development but not for axillary meristem development.

134

135

136

137

138

## 139 RESULTS AND DISCUSSION

140

### 141 Isolation and genetic characterization of *cul2* suppressor mutants

142 The barley *cul2* mutant rarely makes tillers due to its inability to produce axillary buds  
143 (Fig. 1; Babb and Muehlbauer, 2003). To identify suppressors of the *cul2* mutant phenotype, we  
144 mutagenized the Bowman-*cul2.b-rob1* stock. *Rob1* (*orange lemma*) is a phenotypic marker  
145 tightly linked to *cul2* (Franckowiak et al., 1997). Over 15,000 sodium azide-mutagenized, M<sub>3</sub>  
146 Bowman-*cul2.b-rob1* families were screened for plants that produced tillers and two recessive  
147 suppressor mutants were recovered. The two suppressors proved to be alleles of the previously  
148 described *ELI-A* gene (see below) and were named *eli-a.17* and *eli-a.18*. In Bowman-*eli-a.17*;  
149 *cul2.b-rob1* and Bowman-*eli-a.18*; *cul2.b-rob1* mutant plants, the unicum phenotype of *cul2*  
150 was partially suppressed (Fig. 1). For example, in a greenhouse trial, 28 of 41 Bowman-*eli-a.17*;  
151 *cul2.b-rob1* plants produced one or two tillers with the remaining plants having no tillers, and all  
152 21 Bowman-*eli-a.18*; *cul2.b-rob1* plants had one or more tillers (Supplemental Fig. S1).  
153 Unexpectedly, homozygous mutant *eli-a.18* plants were short with leaves that drooped and  
154 lacked ligules (Fig. 1 and Fig. 2), whereas these traits were not seen in *eli-a.17* plants (Fig. 1 and  
155 Fig. 2).

156 To determine if *eli-a.17* and *eli-a.18* were allelic, seven crosses between Bowman-*cul2.b-*  
157 *rob1/cul2.b-rob1*; *eli-a.17/eli-a.17* and Bowman-*cul2.b-rob1/cul2.b-rob1*; *eli-a.18/eli-a.18* were  
158 made. Tillers were observed on 18 out of 19 F<sub>1</sub> plants, demonstrating that the two suppressors  
159 were allelic (Supplemental Fig. S2). In the F<sub>2</sub> plants, *eli-a.18* mutants exhibited stronger  
160 suppression of *cul2.b* than *eli-a.17*. Bowman-*eli-a.18*; *cul2.b-rob1* mutant plants were liguleless  
161 and developed an average of 2.9 tillers per plant compared with Bowman-*eli-a.17*; *cul2.b-rob1*  
162 that developed ligules and had 0.8 tillers per plant (Supplemental Fig. S1). Finally, the  
163 heteroallelic combination of *eli-a.17/eli-a.18* exhibited an intermediate number of tillers in the  
164 *cul2.b* mutant background, 1.59 tillers/plant, and an intermediate liguleless phenotype (Fig. 2,  
165 Supplemental Fig. S1 and Supplemental Fig. S3).

166 The *eli-a.17* and *eli-a.18* alleles also mapped to the same region on chromosome 2HS.  
167 We mapped *eli-a.17* using the *cul2* suppressor phenotype. The *eli-a.17*; *cul2.b-rob1* line was  
168 crossed with the cultivar Steptoe. The tightly linked *rob1* marker and a CAPS marker for SNP  
169 1\_0964 were used to identify 56 homozygous *cul2.b-rob1/cul2.b-rob1* F<sub>2</sub> plants (Supplemental



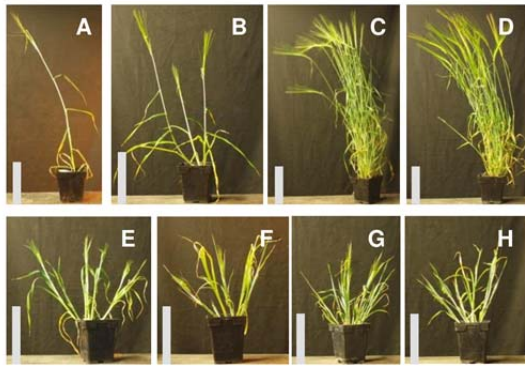


Figure 1: Mutant and non-mutant adult plant characteristics. A, Bowman-*cul2.b-rob1*. B, Bowman-*cul2.b-rob1; eli-a.17*. C, Non-mutant Bowman cultivar. D, Bowman-*eli-a.17*. E, Bowman-*eli-a.18*. F, Bowman-*cul2.b-rob1; eli-a.18*. G, *eli-a.14*. H, *cul2.b-rob1; eli-a.14*. The non-mutant Bowman and Bowman-*eli-a.17* plants in panels C and D were grown in the field and transferred to pots for pictures. Other plants were grown in a growth chamber. Bar = 20 cm.

170 Table S1). The *eli-a.17* phenotype of these 56 individuals was determined in F<sub>3</sub> families,  
 171 because the suppressor phenotype is not fully penetrant and some F<sub>2</sub> *eli-a.17/eli-a.17; cul2.b-*  
 172 *rob1/cul2.b-rob1* plants were unicum. *Eli-a.17* mapped 2.2 cM proximal of SNP 2\_0964 at map  
 173 position 17.85 on the SNP map (Supplemental Fig. S4). *Eli-a.18* was mapped using the  
 174 liguleless phenotype in 220 F<sub>2</sub> individuals from a cross between Bowman-*eli-a.18; cul2.b-rob1*  
 175 and the cultivar Harrington. The liguleless trait was mapped 1.6 cM proximal to SNP 3\_1284 at  
 176 position 19.47 on 2HS (Supplemental Fig. S4).

177 Barley *eli-a* mutants were previously described as recessive mutations producing a  
 178 phenotype of dwarfed liguleless plants with weak culms that break at the nodes (Lundqvist and  
 179 Frankowiak, 2002). We observed these characteristics in the *eli-a.18* mutant. In addition, the  
 180 attachment of outer tillers to the crown was so poor that tillers leaned outwards (Fig. 1). These  
 181 similarities prompted us to test for allelism between *eli-a.18* and the previously described *eli-a*  
 182 alleles. Six mutants classified as *eligulum* that had been backcrossed into the Bowman  
 183 background were examined (Druka et al., 2011). Genetic stocks carrying three of the mutations  
 184 *eli.12, eli-b.5, and eli-a.216* had few of the reported *eli-a* characteristics nor resembled either of  
 185 our two suppressors and were not pursued. *Eli-a.3, eli-a.9, and eli-a.14* mutant stocks exhibited  
 186 the short stature and liguleless characteristics of plants carrying the *eli-a.18* allele. An adult *eli-*  
 187 *a.14* plant is shown in Figure 1, and the liguleless trait from *eli-a* plants is shown in  
 188 Supplemental Figure S3. Three crosses of *eli-a.18* with *eli-a.3*, two crosses with *eli-a.9*, and one  
 189 cross with *eli-a.14* were made. Ten F<sub>1</sub> plants were produced and they all exhibited short and  
 190 liguleless mutant phenotypes. An example of the heteroallelic combination *eli-a.9/eli-a.18* is  
 191 presented in Supplemental Fig. S2. These results confirm that our *cul2* suppressors are allelic  
 192 with *eli-a* mutants.

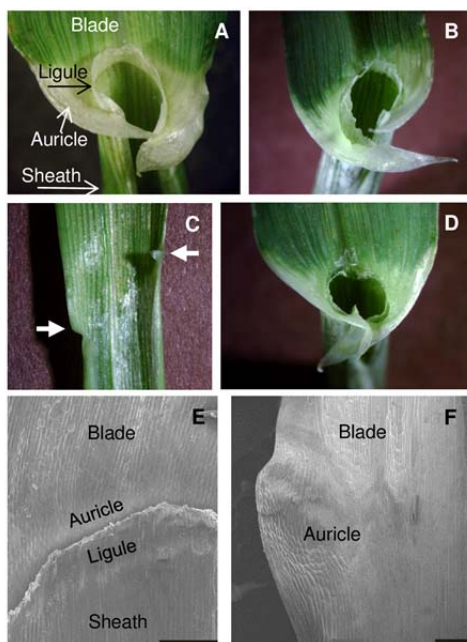


Figure 2: The ligular region in *eli-a* alleles. A – D, Ligules and auricles. A, Non-mutant Bowman. B, Bowman-*eli-a.17*. C, Bowman-*eli-a.18*, note the reduced auricles at the leaf margin, indicated by the arrows and the absence of the ligule. D, Heterozygous Bowman-*eli-a.17/eli-a.18*, note the reduced ligule and auricle development. E – F, scanning electron microscopy of the ligular regions. E, Non-mutant Bowman, the ligule has been trimmed back to uncover the underlying auricle. F, Bowman-*eli-a.18* ligular region. Scale bar = 200  $\mu$ m

193 To determine if *eli-a.3*, *eli-a.9*, and *eli-a.14* suppress the *cul2* unculm phenotype, we  
 194 crossed *eli-a.3*, *eli-a.9*, and *eli-a.14* with Bowman-*cul2.b-rob1*. In total, 23 mutant plants were  
 195 recovered (*eli-a.3/eli-a.3; cul2.b-rob1/cul2.b-rob1*, *eli-a.9/eli-a.9; cul2.b-rob1/cul2.b-rob1*, and  
 196 *eli-a.14/eli-a.14; cul2.b-rob1/cul2.b-rob1*) and 22 of 23 individuals developed tillers. Examples  
 197 of suppression of *cul2.b* by *eli-a.14* and *eli-a.9* are shown in Figure 1 and Supplemental Figure  
 198 S2. All five *eli-a* alleles tested suppress *cul2*, thereby establishing a role for *ELI-A* in axillary  
 199 meristem development.

200

### 201 Axillary bud and tiller development in *eli-a* mutants

202 To study the impact of *eli-a* on early axillary bud development, we examined seven-day-  
 203 old shoot apices from Bowman-*eli-a.17; cul2.b-rob1*, Bowman-*cul2.b-rob1*, Bowman-*eli-a.17*,  
 204 and the non-mutant Bowman cultivar. Despite being a weak allele, the *eli-a.17* allele was used  
 205 for this experiment because germination rates were higher and growth more uniform than other  
 206 *eli-a* alleles. Two to three primary axillary buds were typically seen in non-mutant Bowman  
 207 seedlings at seven days (Fig. 3). In these experiments, no axillary buds were seen in *cul2.b*  
 208 seedlings (Fig. 3), but in previous experiments occasionally an axillary meristem would develop  
 209 but would be blocked from forming an axillary bud (Babb and Muehlbauer, 2003). One to two  
 210 primary axillary buds were present in seven-day-old Bowman-*eli-a.17* seedlings (Fig. 3). In the

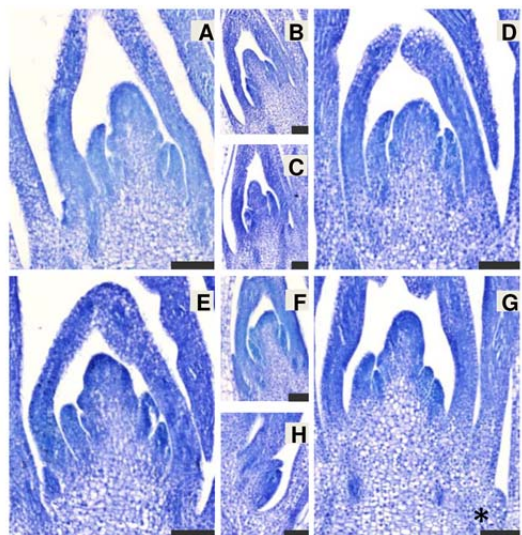


Figure 3. Longitudinal sections of seven-day-old shoot apices from non-mutant and mutant lines stained with Toluidine Blue. Axillary buds are shown in their own panels as median sections of the shoot apex generally do not capture the axillary buds. A, Non-mutant Bowman shoot apical meristem. B, Bowman axillary bud #3. C, Bowman axillary bud #2. D, Bowman-*cul2.b-rob1* shoot apical meristem. E, Bowman-*eli-a.17* shoot apical meristem. F, Bowman-*eli-a.17* axillary bud. G, Bowman-*eli-a.17; cul2.b-rob1* shoot apical meristem, the edge of a small axillary bud is visible at the lower right (\*). H, Section through axillary bud #1 seen in panel G. Size bar = 100  $\mu$ m.

211 Bowman-*eli-a.17; cul2.b-rob1* material, zero to two axillary buds were visible at seven days (Fig.  
 212 3). A seven-day-old Bowman-*eli-a.18* shoot apex is shown in Supplemental Figure S5 for  
 213 comparison.

214 The rates of axillary bud and tiller development between the *eli-a.17* mutant and non-  
 215 mutant were compared, and the numbers of tillers on adult plants for *eli-a.17* were compared to  
 216 the non-mutant. Developing axillary buds and tillers were counted weekly in dissected seedlings  
 217 of *eli-a.17* and non-mutant plants at two weeks through six weeks after planting. Over this  
 218 period, the rate of axillary bud and tiller emergence was significantly slower in *eli-a.17* plants  
 219 than in non-mutant plants (Supplemental Fig. S6).

220 Tiller numbers on field-grown plants were determined for both Bowman-*eli-a.17* and  
 221 Bowman-*eli-a.18* plants. At maturity, plants carrying the strong mutant allele, *eli-a.18* had  
 222 approximately half as many tillers as non-mutant plants, whereas plants carrying the weak *eli-*  
 223 *a.17* allele had approximately 20% fewer tillers than non-mutant plants (Table 1). This small  
 224 reduction in tillering in *eli-a.17* compared to non-mutant Bowman was consistent with tiller  
 225 numbers counted from individual families in previous seasons. For example, non-mutant  
 226 Bowman plants had an average of 45.5 (S.E. = 3.40) tillers per plant and an adjacent family of  
 227 Bowman-*eli-a.17* plants had 33.9 (S.E. = 3.41) tillers per plant in the 2013 field. The reduced  
 228 tiller number in *eli-a.17* and *eli-a.18* mutants compared to non-mutant and the increase in tiller  
 229 number in *cul2.b, eli-a double* mutants indicates that the mechanism controlling rate of tillering

230 and adult tiller number is not necessarily the same mechanism that suppresses the *cul2* mutant  
231 phenotype.

### 232 233 **Ligule and auricle development in *eli-a* mutants**

234 The grass leaf sheath–blade boundary is marked by two structures, the ligule and auricle  
235 (Fig. 2). The auricle can be divided into two parts, a band of small, light colored cells separating  
236 the blade from the sheath and a flap of tissue growing out from the leaf margin that often wraps  
237 around the stem (Fig. 2). The boundary runs perpendicular to the long axis of the leaf, and the  
238 paired auricle flaps are usually directly opposite of each other.

239 Ligules and the bands of auricle cells were generally not visible in *eli-a.18* plants, but  
240 small auricle flaps were present (Fig. 2). Figure 2 presents an adaxial view of the ligular region  
241 from a non-mutant plant with the ligule cut away to show the underlying auricle cells. A small  
242 auricle develops in *eli-a.18* plants at the leaf margin and extends a short distance inward (Fig. 2;  
243 Supplemental Fig. S3). Ligules were not obvious in most plants, although small rudimentary  
244 ligules have been seen. When present, rudimentary ligules were short and did not span the width  
245 of the leaf (Supplemental Fig. S3).

246 A range of ligule and auricle development was seen in the five *eli-a* alleles. Ligule and  
247 auricle development was visibly disrupted in *eli-a.3*, *eli-a.9*, *eli-a.14*, and *eli-a.18* leaves  
248 (Supplemental Fig. S3). Ligules and auricles appeared normal in homozygous *eli-a.17* plants  
249 (Fig. 2 and Supplemental Fig. S3). However, heterozygous *eli-a.17/eli-a.18* plants have small  
250 ligules, while heterozygous *eli-a.18/ELI-A* plants produce normal ligules indicating that the *eli-*  
251 *a.17* allele is not equivalent to the non-mutant allele for ligule development (Fig. 2 and  
252 Supplemental Fig. S3).

253 Another characteristic of leaf development in *eli-a* mutants was the displacement of the  
254 blade–sheath boundary as indicated by the placement of auricle flaps at the leaf margin  
255 (Supplemental Fig. S3). In non-mutant plants, these structures are opposite one another on the  
256 leaf, and the blade–sheath boundary runs approximately perpendicular to the longitudinal axis of  
257 the leaf (Fig. 2 and Supplemental Fig. S3). Displacement of the blade–sheath boundary was  
258 commonly observed in *eli-a.3*, *eli-a.9*, *eli-a.14*, and *eli-a.18* (Supplemental Fig. S3). This  
259 aberrant boundary positioning was infrequent with non-mutant and *eli-a.17* leaves.

260

261 **Inflorescence development**

262 *Eli-a* mutant spikes have a compact appearance with spikelets packed tightly together,  
263 particularly towards the tip (Supplemental Fig. S7; Lundqvist and Franckowiak, 2002). This  
264 characteristic is less obvious in weaker alleles like *eli-a.3* and *eli-a.17* (Supplemental Fig. S7).  
265 The *cul2* mutation produces spikes with spikelets irregularly placed along the spike, particularly  
266 near the tip (Babb and Muehbauer, 2003). Expression of these traits in double mutant *eli-a*;  
267 *cul2.b* plants range from compact spikes with an irregular arrangement of spikelets to severe  
268 disruption of spikelet formation (Supplemental Fig. S7). Thus, although the *eli-a* mutation  
269 partially suppresses the axillary meristem defect in *cul2* mutants, the *cul2* spike phenotype is not  
270 suppressed.

271  
272 **Secondary cell wall defects in *ELI-A* mutants**

273 Non-mutant leaves from the Bowman cultivar have midrib, leaf margin, and bundle  
274 sheath extension cells with thick secondary cell walls providing strength to the leaves. Stained  
275 with Safranin O, these cells appeared small with thick red cell walls (Fig. 4). Corresponding cells  
276 in Bowman-*eli-a.18* leaves were larger with thin cell walls (Fig. 4). Safranin O stains lignin, and  
277 the weaker staining seen in *eli-a.18* suggests reduced lignin content in *eli-a.18* (Ruzin, 1999).  
278 These changes may explain the lack of structural strength and tendency to droop downward in  
279 mutant leaves (Fig. 4). *ELI-A* apparently has a similar function in other tissues. Epidermal cells  
280 in the culm and cells immediately under the epidermis have thick cell walls in non-mutant plants  
281 (Supplemental Fig. S8). The corresponding cells from *eli-a.18* and *eli-a.3* mutant culms have  
282 thin cell walls (Supplemental Fig. S8). This may explain the weakness reported in *eli-a* culms  
283 (Lundqvist and Franckowiak, 2002). However, secondary cell walls did develop in the xylem  
284 and other cells within vascular bundles in *eli-a.18* mutant plants, demonstrating that *ELI-A* is not  
285 an absolute requirement for secondary wall development (Fig. 4).

286 Disrupting cell wall development may explain other characteristics of *eli-a* mutants. In  
287 *eli-a.18* mutant plants, secondary cell wall formation in the mestome sheath and bundle sheath  
288 extensions was greatly reduced. Structural strength is but one function of secondary cell walls  
289 (reviewed in Leegood, 2008). Fricke (2002) proposed that the bundle sheath regulates the flow  
290 of water and photosynthate between the leaf mesophyll and the vascular system. Other work  
291 suggests bundle sheath extensions are an adaptation for desiccation stress (Kenzo et al., 2007).



Figure 4. Secondary cell wall development. A, Comparison of leaves from mature non-mutant Bowman and Bowman-*eli-a.18* plants. B-G are Safranin-O stained. B, Midrib from non-mutant plant. C, Midrib from Bowman-*eli-a.18* plant. D, Leaf vein from non-mutant plant. E, Leaf vein from Bowman-*eli-a.18* plant. F, Leaf margin from non-mutant plant. G, Leaf margin from Bowman-*eli-a.18* plant. Arrows point to cell wall differences in the leaf midrib (B, C), the bundle sheath extension and mestome sheath (D, E), and the leaf margin (F, G). Scale bar = 100  $\mu$ m.

292 Physiological limitations imposed by mutant cell walls could explain the semi-dwarf stature and  
 293 reduced rate of tillering in *eli-a* plants, but would not account for the suppression of the *cul2*  
 294 axillary meristem trait. However, cell wall stiffness in the shoot apex influences auxin transport,  
 295 *CUC3* expression, and leaf primordia emergence in other systems and provides a plausible  
 296 mechanism for controlling axillary meristem development (Kierzkowski et al., 2012; Nakayama  
 297 et al., 2012; Fal et al., 2016).

298

### 299 Isolation and characterization of the *ELI-A* gene

300 The *ELI-A* gene was identified by comparing the transcriptomes of the sodium azide-  
 301 generated *eli-a.17* and *eli-a.18* mutant alleles against non-mutant plants. RNA was isolated and  
 302 sequenced from two-week-old seedling crown tissue from Bowman, Bowman-*cul2.b*, Bowman-  
 303 *cul2.b-rob1*, Bowman-*eli.a-17*, Bowman-*cul2.b-rob1; eli.a-17*, Bowman-*eli.a.18* and Bowman-  
 304 *cul2.b-rob1; eli.a.18*. *De novo* assembly of sequence reads from the Bowman line produced  
 305 31,976 transcripts (Supplemental Data S1). SNPs were then identified between non-mutant  
 306 Bowman and the mutant lines. These SNPs would include any existing variation in the Bowman  
 307 lines and mutations induced by the sodium azide treatment, including the causative mutations for

308 *eli-a.17* and *eli-a.18* (Supplemental Tables S2–S7). Transcript11292 (Supplemental Data S1)  
309 contained a SNP at position 1103 from the Bowman-*cul2.b-rob1; eli-a.17* and Bowman-*eli.a-17*  
310 lines and a different SNP at position 796 in the Bowman-*cul2.b-rob1; eli-a.18* and Bowman-*eli-*  
311 *a.18* lines (Supplemental Tables S2–S5). These two SNPs in Transcript11292 were not present  
312 in the Bowman, Bowman-*cul2.b-rob1* progenitor line, or the related Bowman-*cul2.b* line,  
313 providing evidence that the sequence differences were not pre-existing polymorphisms  
314 (Supplemental Tables S6, S7). Both SNPs were confirmed by Sanger sequencing PCR products  
315 from the Bowman, Bowman-*cul2.b-rob1; eli-a.17* and Bowman-*cul2.b-rob1; eli-a.18* genomic  
316 DNAs.

317 A full-length cDNA sequence, AK375036, matching Transcript11292 was identified in a  
318 BLASTn search of the GenBank non-redundant sequence database. The entire predicted coding  
319 region of AK375036 was sequenced from the *eli-a.17*, *eli-a.18*, *eli-a.3*, *eli-a.9*, and *eli-a.14*  
320 alleles (Fig. 5). Foma, the progenitor allele of *eli-a.3* and *eli-a.9*, Kristina, the progenitor allele  
321 of *eli-a.14*, the Bowman-*cul2.b-rob1* line, progenitor of *eli-a.17* and *eli-a.18*, and the backcross  
322 parent Bowman were also sequenced. *Eli-a.3*, *eli-a.9*, and *eli-a.17* contained the non-  
323 conservative amino acid substitutions proline to serine, threonine to isoleucine, and aspartic acid  
324 to a tyrosine, respectively. The *eli-a.14* and *eli-a.18* alleles contained nonsense mutations. This  
325 cDNA corresponds to gene model MLOC\_58453 from the barley genome (International Barley  
326 Genome Consortium, 2012).

327 MLOC\_58453 co-segregated with the liguleless phenotype in the *eli-a.18* mutant and the  
328 *eli-a.17* suppressor phenotype in the mapping populations described above. MLOC\_58453 was  
329 mapped in the Bowman-*cul2.b-rob1; eli-a.18* Harrington F<sub>2</sub> population using a CAPS marker  
330 targeting the mutated base pair (Supplemental Table S1). As expected, all liguleless plants were  
331 homozygous for the mutant MLOC\_58453 CAPS allele (Supplemental Fig. S4). Similarly, a  
332 SNP located within the MLOC\_58453 coding region co-segregated with the suppressor  
333 phenotype in the *eli-a.17* mapping population (Supplemental Fig. S4 and Supplemental Table  
334 S1). MLOC\_58453 has been mapped to chromosome 2HS on the barley genome assembly (The  
335 International Barley Genome Consortium, 2012).

336

337 ***ELI-A* is a conserved plant gene containing a RNaseH-like domain**

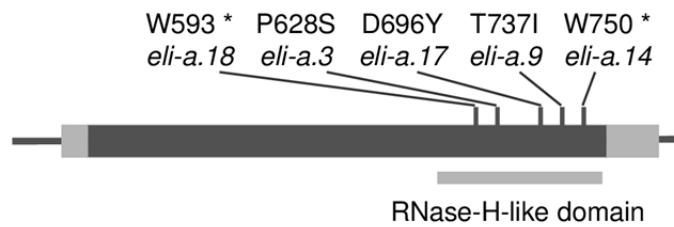


Figure 5. The *ELI-A* gene and location of mutations. The dark grey box indicates the single exon in the gene, and lighter grey boxes mark the 5' and 3' untranslated regions. Mutations in *eli-a.14* and *eli-a.18* created stop codons. Prediction programs Phyre<sup>2</sup>, LOMETS, and InterProScan 5 identified a RNaseH-like domain at the carboxy end of the peptide.

338 Homologous *ELI-A* sequences were found in land plants ranging from *Arabidopsis*  
 339 *thaliana* and rice, to the non-vascular and primitive vascular plants, *Physcomitrella patens* and  
 340 *Selaginella moellendorffii* (Supplemental Table S8). A distantly related sequence was present in  
 341 the green algae *Chlamydomonas reinhardtii*. Mutant phenotypes in *Arabidopsis thaliana* have  
 342 not been reported in TAIR, and the two homologs, AT1G12380 and AT1G62870, are described  
 343 as hypothetical proteins (<https://www.arabidopsis.org/>, May 2017). Nor are the maize gene  
 344 models homologous with *ELI-A* associated with a maize phenotype or classical gene  
 345 (<http://maizegdb.org/>, May 2017). A phylogenetic tree developed from these sequences is  
 346 presented in Supplemental Figure S9. Despite the sequence conservation there is a lack of  
 347 evidence for *ELI-A* function outside of barley.

348 We examined peptide sequences of the barley *ELI-A* protein and in homologous rice and  
 349 *Arabidopsis* proteins. The peptides from barley, rice, and *Arabidopsis* were predicted by Phyre<sup>2</sup>,  
 350 LOMETS, and InterProScan 5 to contain a ribonuclease H-like domain (Kelley and Sternberg,  
 351 2009; Wu and Zhang, 2007; Quevillon et al., 2005). InterProScan 5 did provide additional  
 352 details, but Phyre<sup>2</sup> and LOMETS identified the putative ribonuclease H-like domain as a member  
 353 of the Hermes transposase class. The Hermes class of RNaseH-like domains is found in hAT



354 family transposons; hAT family transposons also contain an N-terminal BED-type zinc finger  
355 and the hAT domain (Hickman et al., 2005).

356 Further examination of the relationship of the *ELI-A* protein to members of the RNase H-  
357 like superfamily found that the Hermes domain is a class I RNaseH that is within clade B under  
358 the classification scheme of Majorek et al. (2014). This family is mainly composed of  
359 transposases with endonuclease activity, although one member of clade B encodes the human  
360 P52<sup>rIPK</sup> protein that regulates a human RNA-dependent serine/threonine protein kinase (Gale et  
361 al., 2002). Phyre<sup>2</sup> detected BED-type zinc fingers in the rice and Arabidopsis peptides with  
362 moderate confidence. However, the hAT domain was not detected by Phyre<sup>2</sup>, LOMETS, or  
363 InterProScan 5 in barley, rice or Arabidopsis. At present, the origin of *ELI-A* from a transposon  
364 is not known.

365

### 366 ***ELI-A* expression pattern**

367 Expression levels of *ELI-A* from eight tissues were calculated from previously published  
368 RNAseq data (The International Barley Genome Consortium, 2012). At this level of resolution,  
369 expression was highest in 5 and 15 mm long immature inflorescences (Supplemental Fig. S10).  
370 *ELI-A* expression levels were low in most other tissues. RNA was extracted from axillary buds,  
371 5-mm long inflorescences, and leaf blades for RT-qPCR to validate the RNAseq data. Transcript  
372 levels were highest in the inflorescence, while transcript levels were below the threshold of  
373 detection in leaf tissue consistent with results from the RNAseq data (Supplemental Fig. S10).

374 RNA *in situ* hybridizations were performed to further refine the distribution of *ELI-A*  
375 transcripts. In non-mutant, four-day-old shoot apices, expression was strong in leaf midribs,  
376 along the leaf margin, the bundle sheath surrounding vascular bundles, and in bundle sheath  
377 extension cells (Fig. 6). A sense control is shown in Supplemental Figure S11. *ELI-A* transcripts  
378 were detected in similar locations in *cul2.b* mutant seedlings (Fig. 6). In transverse *cul2.b*  
379 sections, expression was detected in small clusters of cells along the abaxial leaf surface (Fig. 6).  
380 Expression at this location was variable and was also seen in non-mutant plants (Supplemental  
381 Fig. S11). There were no consistent differences in expression between non-mutant and *cul2.b*  
382 plants.

383 *ELI-A* transcripts are present in developing ligules. A low level of *ELI-A* transcripts was  
384 found in emerging ligules (Fig. 6 and Supplemental Fig. S11), but not in older ligules (Fig. 6).

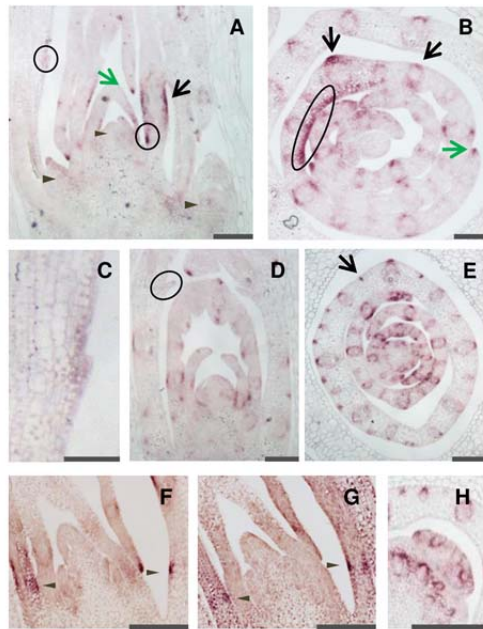


Figure 6. *ELI-A* expression in non-mutant and *cul2.b* seedlings. A-C, Four-day-old non-mutant shoot apex probed with an antisense *ELI-A* probe. A, Longitudinal section showing little staining in or adjacent to the shoot apical meristem and axillary buds, indicated by triangles. Short patches of staining at the adaxial and abaxial sides of leaves were occasionally seen (dark arrow); this pattern is likely from vascular bundles as seen in panels B and H. Staining was observed in newly forming ligules and leaf primordia that may represent developing ligules (circled). Leaf margins were also stained (green arrow). B, Transverse section showing staining in leaf margins, midribs, and around vascular bundles. Staining along a portion of the adaxial side of a developing leaf, circled, can be followed across the leaf in serial sections, and may be associated with the developing ligules. C, Close-up view of ligule circled in panel A. D-E, four-day-old *cul2.b* shoot apex probed with an antisense *ELI-A* probe. D, Longitudinal section of a *cul2.b* shoot. E, Transverse section of a *cul2.b* shoot. *ELI-A* staining pattern was similar to non-mutant shoot apices; the variable staining in small clusters of cells along the abaxial leaf surface (arrow) was seen in non-mutant plants (Supplemental Fig. S11); transcript was not detected in the older ligules (circled). F – G, Serial sections of four-day-old shoot probed for *ELI-A* or *HvLg1*. F, *ELI-A* staining was observed in the same location as the adaxial *HvLg1* staining. G, *HvLg1* staining was detected on the adaxial and abaxial surfaces. H, *ELI-A* expression in leaf axils and axillary buds is associated with vascular bundles. Scale bar = 100  $\mu\text{m}$  in panel C, and 200  $\mu\text{m}$  in other panels.

385 In younger leaf primordia, a prominent signal was present slightly above the base of leaf  
 386 primordia on the adaxial side in longitudinal sections. This signal appeared to correspond to the  
 387 band of expression found on the adaxial surface of leaf primordia in transverse sections (Fig. 6).  
 388 A serial section from higher up along this shoot apex showed expression continuing along the  
 389 adaxial surface (Supplemental Fig. S11). This is the expected location of the preligule band,  
 390 which marks the boundary between the blade and sheath. To verify this, we looked at the  
 391 expression of the barley homolog of the maize *Liguleless1* (*Lg1*) gene. The maize *Lg1* gene is  
 392 expressed at the preligule band at the blade–sheath boundary (Moon et al., 2013). *ELI-A* and  
 393 *HvLGI* transcripts were both found on the adaxial surface of the blade–sheath boundary in serial  
 394 sections from the same shoot apex (Fig. 6). A *HvLGI* sense control is shown in Supplemental  
 395 Figure S11. Taken together, these results indicate that *ELI-A* acts like a boundary gene in the  
 396 development of the blade–sheath boundary.

397 Weak staining was sometimes seen in axillary buds and in leaf axils adjacent to  
 398 developing axillary meristems, as well as within axillary buds in longitudinal sections (Fig. 6 and

399 Supplemental Fig. S11). In transverse sections, this transcript appeared to associate with  
400 developing vascular bundles rather than the leaf axil or axillary meristem (Fig. 6). *ELI-A*  
401 expression further down the shoot apex where the axillary bud emerged from the shoot apex was  
402 very weak compared to expression around vascular bundles higher up the shoot apex  
403 (Supplemental Fig. S11). The expression pattern of *ELI-A* did not indicate a direct function in  
404 boundary formation or stem cell maintenance.

405 Sclerenchyma cells are found in developing leaf ribs, hypodermal sclerenchyma cells,  
406 and leaf margins from barley plants (Wenzel et al., 1997; Trivett and Evert, 1998). These are  
407 locations where *ELI-A* transcripts were detected in leaf primordia. In *eli-a.18* mutants, cells  
408 comprising midribs have thin cell walls and lack the thick secondary cell walls of normal rib  
409 cells. Elsewhere in the leaf and in the culm, *ELI-A* transcripts coincided with cells having  
410 thickened secondary cell walls (Fig. 5 and Fig. 6). *ELI-A* transcripts were not detected in the  
411 xylem or phloem (Fig. 6 and Supplemental Fig. 11). This absence of secondary cell walls can  
412 explain the weak leaves and culms in *eli-a* mutant plants. However, the absence of *ELI-A*  
413 transcripts in leaf axils from both *CUL2* and *cul2.b* plants argues against a direct role for  
414 secondary cell walls in the suppression of the *cul2* tillering phenotype by *eli-a*.

415

#### 416 ***ELI-A* acts like a boundary gene in the leaf but not in the leaf axil**

417 A conserved set of genes are believed to control leaf and axillary meristem development.  
418 In tomato and other eudicots, development of leaf serrations, leaflets, and axillary meristems in  
419 leaf axils are regulated by *CUC*, *RAX*, and *LATERAL SUPPRESSOR* (Busch et al., 2011). Grass  
420 leaves lack serrated margins and leaflets common in eudicots, but there is a boundary between  
421 the blade and sheath consisting of the ligule and auricles (Langdale, 2005; Lewis and Hake,  
422 2015). Laser microdissection transcriptome analysis showed maize *CUC2*, *BOP*, and *ELI-A*  
423 homologs upregulated at the blade–sheath boundary (Johnston et al., 2014). *In situ*  
424 hybridizations confirmed the maize *CUC2* and *BOP* expression in newly forming ligules at the  
425 leaf blade - sheath and axillary meristem boundaries (Johnston et al., 2014). Barley *CULA* and  
426 maize *BOP* are homologous genes. This postulated genetic system may derive from a common  
427 evolutionary origin for leaves and axillary meristems as suggested by Busch and colleagues  
428 (2011), and is consistent with expectations from the barley phytomer model proposed by Forster

429 and co-workers (2011). Alternatively, the conserved genes may be part of a conserved genetic  
430 module that acts in leaf and axillary meristem development (Carroll, 2008).

431 This system of genes is expected to function in barley development. The barley *BOP*  
432 homolog, *CULA*, is expressed in newly formed ligules at the blade–sheath junction and at  
433 axillary meristem boundaries in leaf axils (Tavakol et al., 2015). However, *CULA* is expressed in  
434 developing ligules and does not appear to specify the location of the blade-sheath boundary  
435 (Tavakol et al., 2015). Like *CULA*, *ELI-A* is expressed in newly forming ligules, but is also  
436 expressed earlier in development than *CULA* where its expression pattern overlaps the barley  
437 homolog of the maize *Lg1* gene in the preligular region separating the blade from sheath (Moon  
438 et al., 2013). In addition, the *ELI-A* mutants (*eli-a.9*, *eli-a.3*, *eli-a.14* and *eli-a.18*) exhibiting a  
439 liguleless phenotype also exhibit a disrupted blade–sheath boundary (Supplemental Fig. S3).  
440 Taken together, our results show that *ELI-A* and *CULA* are both necessary to produce a ligule,  
441 with *ELI-A* acting at a similar time and place with *HvLg1* to establish the leaf blade–sheath  
442 boundary.

443 *CULA* and *ELI-A* both have roles in axillary meristem development. However, their roles  
444 in axillary development appear different because the *cul4* and *eli-a* tillering phenotypes share  
445 few characteristics. The *cul4* mutation restricts axillary meristem development to a short  
446 developmental window; new axillary buds cease appearing after three to four weeks in *cul4.5*  
447 plants (Tavakol et al., 2015). The *eli-a* mutation slows the rate of axillary meristem development.  
448 Furthermore, *eli-a* mutants suppress the low-tillering *cul2* phenotype; *cul4* does not (Babb and  
449 Muehlbauer, 2003).

450 RNA *in situ* hybridization provided further evidence for differing roles for *ELI-A* during  
451 leaf and axillary branch development. The *ELI-A* transcripts were present at the leaf blade–  
452 sheath boundary where it participates in ligule development. Although *ELI-A* transcripts were  
453 occasionally detected in or adjacent to developing axillary buds in longitudinal sections, *ELI-A*  
454 was shown in transverse sections to be closely associated with vascular bundles rather than organ  
455 boundaries or meristematic regions. This expression pattern in the leaf axil was not similar to  
456 other characterized axillary meristem boundary genes including *CULA* and the rice *CUC3* and  
457 *RA2* homologs (Tavakol et al., 2015; Oikawa and Kyozyuka, 2009). It is possible that transient  
458 *ELI-A* expression in axillary meristems or organ boundaries was not detected, or the *ELI-A*  
459 protein is transported as shown for the rice *LAX* protein (Oikawa and Kyozyuka, 2009). While

460 acknowledging these possibilities, our data support a model where *ELI-A* has an early role and  
461 *CULA* has a later role in creating the blade–sheath boundary during leaf development. However,  
462 during axillary meristem development, *CULA* is expressed in the leaf axil and plays a role in  
463 boundary formation. While *ELI-A* does not appear to be expressed in the leaf axil boundary, it  
464 still has a role in axillary meristem development. Taking these findings together, we propose that  
465 *ELI-A* acts like a boundary gene at the leaf blade-sheath boundary and promotes secondary cell  
466 wall formation in leaves and other tissues, but acts in an unknown manner during axillary  
467 meristem development.

468

469

## 470 MATERIALS AND METHODS

### 471 Plant materials and populations:

472 Mutant alleles *cul2.b*, *eli-a.3*, *eli-a.9*, *eli-a.14*, and *rob1* were obtained from the collection  
473 of mutants backcrossed to the cultivar Bowman (Druka et al., 2011). Plants were either field  
474 grown, or grown under controlled conditions in a greenhouse or growth chamber with 16 hours  
475 of light at 22 °C and 8 hours dark at 18 °C. Supplemental Table S9 provides information on the  
476 mutant alleles and barley cultivars used here.

477 The *cul2* suppressor screen was conducted by mutagenizing Bowman-*cul2.b-rob1* grain.  
478 The *rob1* allele is approximately 2 cM from *cul2* and produces an orange lemma phenotype that  
479 was used to track the tightly linked *cul2.b* allele. Approximately 20,000 Bowman-*cul2.b-rob1*  
480 kernels were treated with sodium azide according to the protocol described in Döring et al.  
481 (1999). From the M<sub>2</sub> plants, over 15,000 M<sub>3</sub> families (~70,000 plants) were produced and  
482 screened. M<sub>3</sub> families segregating for plants with tillers were identified. Families were re-tested  
483 for the suppressor phenotype in subsequent generations.

484 To recover homozygous *eli-a.17* plants, we conducted a single backcross of *eli-a.17/eli-*  
485 *a.17; cul2.b-rob1/cul2.b-rob1* plants to the non-mutant Bowman cultivar and self-pollinated an  
486 F<sub>1</sub> plant to generate an F<sub>2</sub> population. Families derived from phenotypically non-mutant F<sub>2</sub>  
487 plants were screened in the F<sub>3</sub> and F<sub>4</sub> generations to recover homozygous *eli-a.17/eli-a.17* and  
488 *eli-a.17/eli-a.17; cul2.b-rob1/cul2.b-rob1* lines (Supplemental Fig. S12). *Eli-a.18* mutant plants  
489 were identified by their short stature and liguleless leaves. F<sub>2</sub> populations segregating *eli-a.17*  
490 and *eli-a.18* were produced by crossing the Bowman-*eli-a.18; cul2.b-rob1* line with the non-  
491 mutant cultivar Harrington, and by crossing the Bowman-*eli-a.17; cul2.b-rob1* line with the non-  
492 mutant cultivar Steptoe.

493 Seedling tests for suppression of *cul2.b* by *eli-a.3*, *eli-a.9*, and *eli-a.14* were performed  
494 by crossing the mutants and recovering *eli-a/+; cul2.b/cul2.b* individuals. These plants were  
495 allowed to self-pollinate. Tillering phenotypes of suppression of *cul2* by *eli-a.3* and *eli-a.14*  
496 were scored in the growth chamber in three to four-week-old F<sub>2</sub> plants. Suppression of *cul2.b* by  
497 *eli-a.9* was tested in field grown F<sub>2</sub> families.

498

### 499 Morphological characterization

500 Shoot apices from one-week-old seedlings were sectioned and stained to examine axillary  
501 bud development as previously described (Babb and Muehlbauer, 2003). Axillary buds and  
502 tillers were counted on growth chamber grown plants, weeks two through six. Three replicates,  
503 three plants per replication, were counted at each time point; at least eight plants were examined  
504 in all but two time points. Leaves were removed to count axillary buds and tillers. Axillary buds  
505 were further classified as primary axillary buds, those growing in leaf axils, and secondary  
506 axillary buds, those growing in tiller axils (Dabbert et al., 2010). Tiller number was determined  
507 from field grown plants at four weeks, six weeks, and at maturity; five plants per replicates with  
508 six replicates of non-mutant and Bowman-*eli-a.17*, and five replicates of Bowman-*eli-a.18* were  
509 randomized in the field.

510 Ligular regions were examined on four to six-week-old plants grown in the growth  
511 chamber or greenhouse. Development of ligules, auricles, and other features were characterized  
512 from the second or third leaf. The leaf blade–sheath junction region was photographed under  
513 low-power light microscopy and with cryo-scanning electron microscopy. Scanning electron  
514 microscopy was performed on a Hitachi S3500N scanning electron microscope at 5 or 10 kV  
515 (Ahlstrand, 1996).

516 For histological work, plant tissues were fixed in paraformaldehyde and embedded in  
517 paraffin (Javelle et al., 2011). Sections were stained with Toluidine Blue or Safranin O  
518 (Humason, 1979; Ruzin, 1999). RNA *in situ* hybridizations were performed as described by  
519 Javelle et al., (2011). Probes for RNA *in situ* hybridizations were developed from PCR  
520 amplicons from genomic DNA using primers ELI-1393F and ELI-1877R or HvLG1-79F and  
521 HvLG1-598R, cloned into pGEM-T Easy (Promega, Madison, WI). Plasmids were used as  
522 templates for PCR with M13 forward and reverse primers. RNA was synthesized from resulting  
523 amplicons with SP6 or T7 RNA polymerase to make the sense and antisense probes using the  
524 Roche DIG RNA Labeling Kit (Sigma-Aldrich, St. Louis, MO).

## 525 **Molecular biology procedures**

526 Procedures for DNA isolation, PCR, Cleavage Amplified Polymorphic Sequence (CAPS)  
527 markers, and other routine molecular techniques were described previously (Dabbert et al.,  
528 2010). PCR primers (Supplemental Table S10) were developed using the program Primer3  
529 (Rozen and Skaletsky 2000). Sanger sequencing was performed by the University of Minnesota

530 Genomics Center. CAPS markers were developed from previously mapped SNP sequences  
531 (Close et al., 2009), and the program JoinMap 4 was used to calculate map distances (Van  
532 Ooijen, 2006).

533 Total RNA for sequencing (RNA-seq) was isolated from crown tissue containing the  
534 shoot apical meristem and axillary meristems from 14-day-old seedlings grown in growth  
535 chambers using the RNeasy Plant Mini Kit (Qiagen). There were three replicates of each  
536 genotype (Bowman, Bowman-*cul2.b*, Bowman-*cul2.b-rob1*, Bowman-*eli.a-17*, Bowman-*cul2.b-*  
537 *rob1; eli.a-17*, Bowman-*eli.a.18* and Bowman-*cul2.b-rob1; eli.a.18*), six seedlings per replicate,  
538 and tissue from each genotype was pooled. Poly A+ RNA isolation, library construction, and  
539 Illumina sequencing were performed by the University of Minnesota Genomics Center.  
540 Fragment sizes for sequencing averaged 200 base pairs (bp), after accounting for adaptor  
541 sequences, and 76 bp, paired-end reads were produced.

542 Relative *ELI-A* expression levels were compared in inflorescence, axillary bud, and leaf  
543 blade tissues by RT-qPCR using the procedure described by Tavakol et al. (2015). Total RNA  
544 was isolated from one cm long axillary buds from two-week-old seedlings, and five mm long  
545 inflorescences, and leaf blades from four-week-old seedlings using the Qiagen RNeasy kit  
546 (Qiagen). Approximately 250 ng of total RNA was DNase treated (RQ1 Rase-Free DNase,  
547 Promega) prior to cDNA synthesis with the ImProm-II Reverse Transcription System (Promega).  
548 One-third of the product was used for PCR. Quantitative PCR was performed on an Applied  
549 Biosystems StepOnePlus Real Time PCR System with the QuantiFast SYBR Green mix  
550 (Qiagen). *GAPDH* and *UBI* were used for normalization (Tavakol et al., 2015). Three  
551 replicates, with three to five plants each, were randomized and grown together in a growth  
552 chamber as described above. Primer sequences are shown in Supplemental Table S10.

553

#### 554 **Sequence assembly pipeline and SNP analysis**

555 Reads for all samples were quality trimmed from both ends with custom Java code, using  
556 a base quality cutoff of Phred 20. Reads shorter than 30 bp were discarded. Trimmed reads  
557 from the Bowman sample were assembled *de novo* using the Trinity transcriptome assembler on  
558 default settings (release r2011-05-13, Grabherr et al., 2011). This resulted in a total of 31,976  
559 transcript sequences (Supplemental Data S1).



560 Trimmed reads from each mutant sample were mapped separately to the Bowman Trinity  
561 transcripts using the Bowtie read mapper v. 0.12.7 (Langmead et al., 2009). To keep  
562 mismapping and the resulting false positive SNPs to a minimum, a strict mismatch rate of 1  
563 mismatch per read was applied. Reads were mapped in “all” mode which allows multi-mappable  
564 reads to map to all of their possible mapping locations. The “--best –strata” parameter was used  
565 to ensure that only the best mapping locations were reported.

566 For each genotype, SNP discovery was carried out using custom-written code  
567 implemented as a prototype feature in Tablet (Milne et al., 2013). The raw variant data was then  
568 filtered using a minor allele frequency of  $\geq 0.9$ , to identify homozygous SNPs with the  
569 Bowman reference sequence only. Several further stages of SNP filtering followed, all of which  
570 were aimed at removing false positive SNPs. First, SNPs that were less than a read’s length  
571 from contig start or end, or regions with zero read coverage, were removed as a large proportion  
572 of these can be assumed to be artifacts caused by mis-assembly of the reference sequence (M.  
573 Bayer, unpublished data). SNPs with fewer than six instances of the alternate allele were also  
574 removed to exclude low coverage, low confidence variants. We called SNPs by mapping the  
575 Bowman reads against the Bowman Trinity assembly as a control set, on the assumption that any  
576 SNPs found in this largely homozygous cultivar must be artifacts caused by read mis-mapping or  
577 mis-assembly of the reference sequence. SNPs discovered in this dataset were subsequently  
578 removed from all of the mutant SNP sets. The remaining ‘robust SNPs’ were used for analysis.

579

## 580 **Accession Numbers**

581 RNAseq data have been deposited into the National Center for Biotechnology  
582 Information Short Read Archive, accession number SRP076379. *ELI-A* sequences were  
583 deposited in the National Center for Biotechnology Information database, accession numbers  
584 KU844110 - KU844117. Additional sequences mentioned in this article can be found in the  
585 GenBank, TAIR, or PlantGDB databases under the following accession numbers:  
586 GenBank/EMBL: Bradi5g04710 (XM\_003581043), Bradi5g04720 (XM\_003579296),  
587 CHLREDRAFT\_180901 (XM\_001692084), LOC\_Os04g19140 (XM\_015779144),  
588 LOC\_Os02g25230 (XM\_015767599), PP1S21\_302V6 (XM\_001756068), PP1S105\_108V6  
589 (XM\_001768660), PP1S226\_73V6 (XM\_001777733), PP1S111\_138V6 (XM\_001769128),  
590 SELMODRAFT\_231485 (XM\_002969799), SELMODRAFT\_10589 (XM\_002985134),  
591 Si009424m.g (XM\_004975201), Si016308m.g (XP\_004952406), Sb04g014800  
592 (XM\_002453721), Solyc08g079550 (XM\_004246091),

593 Solyc03g007180 (XM\_004234118), Zm00001d004164 (XR\_562337), Zm00001d025091  
594 (XM\_008664864), Zm00001d015889 (XM\_008647228), Zm00001d053254 (XM\_008681506);  
595 PlantGDB: Sb06g003790.1; and TAIR: AT1G12380, AT1G62870. Original photographs used  
596 for the figures have been archived at University of Minnesota Data Repository (DRUM) and can  
597 be accessed at <https://doi.org/10.13020/D61H4D>.

598

599

600 **Supplemental Materials**

601 The following materials are available in the online version of this article.

602 **Supplemental Tables**

603 **Supplemental Table S1.** CAPS markers for *eli-a* alleles and mapping.

604 **Supplemental Table S2.** *eli-a.17*; *cul2.b-rob1* SNP list.

605 **Supplemental Table S3.** *eli-a.18*; *cul2.b-rob1* SNP list.

606 **Supplemental Table S4.** *eli-a.17* SNP list.

607 **Supplemental Table S5.** *eli-a.18* SNP list.

608 **Supplemental Table S6.** *cul2.b-rob1* SNP list

609 **Supplemental Table S7.** *cul2.b* SNP list.

610 **Supplemental Table S8.** Homologous *ELI-A* sequences in other species.

611 **Supplemental Table S9.** Plant materials.

612 **Supplemental Table S10.** PCR primer sequences.

613

614

615 **Supplemental Figures**

616 **Supplemental Figure S1.** Suppression of *cul2* by *eli-a.17* and *eli-a.18* promotes tillering.

617 **Supplemental Figure S2.** Genetic testing of *eli-a* alleles.

618 **Supplemental Figure S3.** Ligule development in *eli-a* alleles.

619 **Supplemental Figure S4.** Mapping *eli-a.17* and *eli-a.18* on chromosome 2HS.

620 **Supplemental Figure S5.** Axillary bud development in *Bowman- eli-a.18*.

621 **Supplemental Figure S6.** Rate of axillary bud and tiller appearance.

622 **Supplemental Figure S7.** *Eli-a* spike phenotypes.

623 **Supplemental Figure S8.** Secondary cell wall development in culms.

624 **Supplemental Figure S9.** Phylogenetic tree of *ELI-A* homologs.

625 **Supplemental Figure S10.** *ELI-A* expression data.

626 **Supplemental Figure S11.** *ELI-A in situ* hybridizations.

627 **Supplemental Figure S12.** Crossing scheme to develop *eli-a.17* and *Bowman-cul2.b-*  
628 *rob1*; *eli-a.17* families.

629 **Supplemental Data**

630 **Supplemental Data S1.** RNAseq Transcript list.

631

632

633

634 **ACKNOWLEDGEMENTS**

635 We thank Bruna Bucciarelli for assistance with microscopy; Gail Celio and Grant Barthel at the  
 636 University Imaging Center, University of Minnesota, for help with SEM and light microscopy;  
 637 Kevin Smith for providing field space, Sue Miller for assistance with RT-qPCR, Lin Li and Juan  
 638 Gutierrez-Gonzalez for help with bioinformatics; The Nordic Genetic Resource Center, Harold  
 639 Bockelman, the USDA National Small Grains Collection, and Andris Kleinhofs, Washington  
 640 State University for providing materials; and Jerome Franckowiak for insights on the  
 641 interpretation of mutants. This research was supported by a grant from the United States  
 642 Department of Agriculture-CSREES-NRI Plant Growth and Development program grant # 2004-  
 643 03440 and funds received from the Triticeae Coordinated Agricultural Project, US Department  
 644 of Agriculture/National Institute for Food and Agriculture grant number 2011-68002-30029 to  
 645 G.J.M.

646

647 **Table 1. Tiller development in *eli-a.17* and *eli-a.18* mutants and in non-mutant Bowman.**

Genotype	Tiller Number – 4 weeks	Tiller Number – 6 weeks	Tiller Number – maturity
Bowman <sup>1</sup>	7.69	28.01	33.95
Bowman- <i>eli-a.17</i> <sup>1</sup>	6.70	23.93*	27.37*
Bowman <sup>2</sup>	6.61	27.32	43.99
Bowman- <i>eli-a.18</i> <sup>2</sup>	4.73	15.75*	21.97*

648 <sup>1</sup> 2015 field

649 <sup>2</sup> 2016 field

650 \* t<0.05 two-tailed Student's *t*-test

651

652

653 **Figure legends**

654 Figure 1: Mutant and non-mutant adult plant characteristics. A, Bowman-*cul2.b-rob1*. B,  
655 Bowman-*cul2.b-rob1; eli-a.17*. C, Non-mutant Bowman cultivar. D, Bowman-*eli-a.17*. E,  
656 Bowman-*eli-a.18*. F, Bowman-*cul2.b-rob1; eli-a.18*. G, *eli-a.14*. H, *cul2.b-rob1; eli-a.14*. The  
657 non-mutant Bowman and Bowman-*eli-a.17* plants in panels C and D were grown in the field and  
658 transferred to pots for pictures. Other plants were grown in a growth chamber. Bar = 20 cm.

659

660 Figure 2: The ligular region in *eli-a* alleles. A–D, Ligules and auricles. A, Non-mutant Bowman.  
661 B, Bowman-*eli-a.17*. C, Bowman-*eli-a.18*. Note the reduced auricles at the leaf margin, indicated  
662 by the arrows and the absence of the ligule. D, Heterozygous Bowman-*eli-a.17/eli-a.18*. Note the  
663 reduced ligule and auricle development. E–F, scanning electron micrographs of the ligular  
664 regions. E, Non-mutant Bowman. The ligule has been trimmed back to uncover the underlying  
665 auricle. F, Bowman-*eli-a.18* ligular region. Scale bar = 200  $\mu\text{m}$

666

667

668 Figure 3. Longitudinal sections of seven-day-old shoot apices from non-mutant and mutant lines  
669 stained with Toluidine Blue. Axillary buds are shown in their own panels as median sections of  
670 the shoot apex and generally do not capture the axillary buds. A, Non-mutant Bowman shoot  
671 apical meristem. B, Bowman axillary bud #3. C, Bowman axillary bud #2. D, Bowman-*cul2.b-*  
672 *rob1* shoot apical meristem. E, Bowman-*eli-a.17* shoot apical meristem. F, Bowman-*eli-a.17*  
673 axillary bud. G, Bowman-*eli-a.17; cul2.b-rob1* shoot apical meristem. The edge of a small  
674 axillary bud is visible at the lower right (\*). H, Section through axillary bud #1 seen in panel G.  
675 Scale bar = 100  $\mu\text{m}$ .

676

677 Figure 4. Secondary cell wall development. A, Comparison of leaves from mature non-mutant  
678 Bowman and Bowman-*eli-a.18* plants. B–G are Safranin-O stained. B, Midrib from non-mutant  
679 plant. C, Midrib from Bowman-*eli-a.18* plant. D, Leaf vein from non-mutant plant. E, Leaf vein  
680 from Bowman-*eli-a.18* plant. F, Leaf margin from non-mutant plant. G, Leaf margin from

681 Bowman-*eli-a.18* plant. Arrows point to cell wall differences in the leaf midrib (B, C), the  
682 bundle sheath extension and mestome sheath (D, E), and the leaf margin (F, G). Scale bar = 100  
683  $\mu\text{m}$ .

684

685 Figure 5. The *ELI-A* gene and location of mutations. The dark grey box indicates the single  
686 exon in the gene and lighter grey boxes mark the 5' and 3' untranslated regions. Mutations in  
687 *eli-a.14* and *eli-a.18* created stop codons. Prediction programs Phyre<sup>2</sup>, LOMETS, and  
688 InterProScan 5 identified a RNaseH-like domain at the carboxy end of the peptide.

689

690 Figure 6. *ELI-A* expression in non-mutant and *cul2.b* seedlings. A-C, Four-day-old non-mutant  
691 shoot apex probed with an antisense *ELI-A* probe. A, Longitudinal section showing little  
692 staining in or adjacent to the shoot apical meristem and axillary buds, indicated by triangles.  
693 Short patches of staining at the adaxial and abaxial sides of leaves were occasionally seen (dark  
694 arrow); this pattern is likely from vascular bundles as seen in panels B and H. Staining was  
695 observed in newly forming ligules and leaf primordia that may represent developing ligules  
696 (circled). Leaf margins were also stained (green arrow). B, Transverse section showing staining  
697 in leaf margins, midribs, and around vascular bundles. Staining along a portion of the adaxial  
698 side of a developing leaf, circled, can be followed across the leaf in serial sections, and may be  
699 associated with the developing ligules. C, Close-up view of ligule circled in panel A. D-E, four-  
700 day-old *cul2.b* shoot apex probed with an antisense *ELI-A* probe. D, Longitudinal section of a  
701 *cul2.b* shoot. E, Transverse section of a *cul2.b* shoot. *ELI-A* staining pattern was similar to non-  
702 mutant shoot apices; the variable staining in small clusters of cells along the abaxial leaf surface  
703 (arrow) was seen in non-mutant plants (Supplemental Fig. S11); transcripts were not detected in  
704 the older ligules (circled). F-G, Serial sections of four-day-old shoot probed for *ELI-A* or *HvLg1*.  
705 F, *ELI-A* staining was observed in the same location as the adaxial *HvLg1* staining. G, *HvLg1*  
706 staining was detected on the adaxial and abaxial surfaces. H, *ELI-A* expression in leaf axils and  
707 axillary buds is associated with vascular bundles. Scale bar = 100  $\mu\text{m}$  in panel C and 200  $\mu\text{m}$  in  
708 other panels.

709







## Parsed Citations

Ahlstrand GG (1996) Low-temperature low-voltage scanning microscopy (LTLVSEM) of uncoated frozen biological materials: a simple alternative. In: G Bailey, J Corbett, R Dimlich, J Michael, N Zaluzec, eds, Proceedings of Microscopy Microanalysis. San Francisco Press, San Francisco, pp 918–919

Pubmed: [Author and Title](#)

CrossRef: [Author and Title](#)

Google Scholar: [Author Only](#) [Title Only](#) [Author and Title](#)

Babb S, Muehlbauer GJ (2003) Genetic and morphological characterization of the barley unculm2 (cul2) mutant. Theor Appl Genet 106: 846-857

Pubmed: [Author and Title](#)

CrossRef: [Author and Title](#)

Google Scholar: [Author Only](#) [Title Only](#) [Author and Title](#)

Bar M, Ori N (2014) Leaf development and morphogenesis. Development 141: 4219-4230.

Pubmed: [Author and Title](#)

CrossRef: [Author and Title](#)

Google Scholar: [Author Only](#) [Title Only](#) [Author and Title](#)

Becraft PW, Bongard-Pierce DK, Sylvester AW, Poethig RS, Freeling M (1990) The liguleless-1 gene acts tissue specifically in maize leaf development. Develop Biol 141: 220-232

Pubmed: [Author and Title](#)

CrossRef: [Author and Title](#)

Google Scholar: [Author Only](#) [Title Only](#) [Author and Title](#)

Berger Y, Harpax-Saad S, Brand A, Melnik H, Sirding N, Alvarez JP, Zinder M, Samach A, Eshed Y, Ori N (2009) The NAC-domain transcription factor GOBLET specifies leaflet boundaries in compound tomato leaves. Development 136: 823-832

Pubmed: [Author and Title](#)

CrossRef: [Author and Title](#)

Google Scholar: [Author Only](#) [Title Only](#) [Author and Title](#)

Bilsborough GD, Runions A, Barkoulas M, Jenkins HW, Hasson A, et al (2011) Model for the regulation of Arabidopsis thaliana leaf margin development. Proc. Natl. Acad. Sci. USA 108: 3424-3429

Pubmed: [Author and Title](#)

CrossRef: [Author and Title](#)

Google Scholar: [Author Only](#) [Title Only](#) [Author and Title](#)

Busch BL, Schmitz G, Rossmann S, Piron F, Ding J, Bendahmane A, Theres K (2011) Shoot branching and leaf dissection in tomato are regulated by homologous gene modules. Plant Cell 23: 3595-3609

Pubmed: [Author and Title](#)

CrossRef: [Author and Title](#)

Google Scholar: [Author Only](#) [Title Only](#) [Author and Title](#)

Carroll SB (2008) Evo-devo and an expanding evolutionary synthesis: A genetic theory of morphological evolution. Cell 134: 25-36

Pubmed: [Author and Title](#)

CrossRef: [Author and Title](#)

Google Scholar: [Author Only](#) [Title Only](#) [Author and Title](#)

Close TJ, Bhat PR, Lonardi S, Wu Y, Rostoks N, Ramsay L, Druka A, Stein N, Svensson, JT, Wanamaker S, et al (2009) Development and implementation of high-throughput SNP genotyping in barley. BMC Genomics 10: 582.

Pubmed: [Author and Title](#)

CrossRef: [Author and Title](#)

Google Scholar: [Author Only](#) [Title Only](#) [Author and Title](#)

Dabbert T, Okagaki RJ, Cho S, Heinen S, Boddu J, Muehlbauer GJ (2010) The genetics of barley low-tillering mutants: low number of tillers-1 (Int1). Theor Appl Genet 121: 705-717

Pubmed: [Author and Title](#)

CrossRef: [Author and Title](#)

Google Scholar: [Author Only](#) [Title Only](#) [Author and Title](#)

Dereeper A, Guignon V, Blanc G, Audic S, Buffet S, et al (2008) Phylogeny.fr: robust phylogenetic analysis for the non-specialist. Nucleic Acids Res 36 (Web Server issue): W465-9

Pubmed: [Author and Title](#)

CrossRef: [Author and Title](#)

Google Scholar: [Author Only](#) [Title Only](#) [Author and Title](#)

Döring H-P, Lin J, Urig H, Salamini F (1999) Clonal analysis of the development of the barley (Hordeum vulgare L.) leaf using periclinal chlorophyll chimeras. Planta 207: 335-342

Pubmed: [Author and Title](#)

CrossRef: [Author and Title](#)

Google Scholar: [Author Only](#) [Title Only](#) [Author and Title](#)

Druka A, Franckowiak J, Lundqvist U, Bonar N, Alexander J, et al (2011) Genetic dissection of barley morphology and development.

**Plant Physiol 155: 617-627**

Pubmed: [Author and Title](#)  
CrossRef: [Author and Title](#)  
Google Scholar: [Author Only Title Only Author and Title](#)

**Fal K, Landrein B, Hamant O (2016) Interplay between miRNA regulation and mechanical stress for CUC gene expression at the shoot apical meristem. Plant Signal Behav 11: e1127497**

Pubmed: [Author and Title](#)  
CrossRef: [Author and Title](#)  
Google Scholar: [Author Only Title Only Author and Title](#)

**Forster BP, Franckowiak JD, Lundqvist U, Lyon J, Pitkethly I, Thomas WTB (2007) The barley phytomer. Ann Bot 100: 725-733**

Pubmed: [Author and Title](#)  
CrossRef: [Author and Title](#)  
Google Scholar: [Author Only Title Only Author and Title](#)

**Franckowiak JD, Konishi T, Lundqvist U (1997) BGS 254, Orange lemma, rob. Barley Genet Newsl 26: 235-236**

Pubmed: [Author and Title](#)  
CrossRef: [Author and Title](#)  
Google Scholar: [Author Only Title Only Author and Title](#)

**Fricke W (2002) Biophysical limitation of cell elongation in cereal leaves. Ann Bot 90: 157-167**

Pubmed: [Author and Title](#)  
CrossRef: [Author and Title](#)  
Google Scholar: [Author Only Title Only Author and Title](#)

**Gale Jr M, Blakely CM, Darveau A, Romano PR, Korth, MJ, and Katze MG (2002) P52rIPK regulates the molecular cochaperone P58IPK to mediate control of the RNA-dependent protein kinase in response to cytoplasmic stress. Biochemistry 41: 11878-11887**

Pubmed: [Author and Title](#)  
CrossRef: [Author and Title](#)  
Google Scholar: [Author Only Title Only Author and Title](#)

**Gallavotti A, Zhao Q, Kyoizuka J, Meeley RB, Ritter MK, et al (2004) The role of barren stalk1 in the architecture of maize. Nature 432: 630-635**

Pubmed: [Author and Title](#)  
CrossRef: [Author and Title](#)  
Google Scholar: [Author Only Title Only Author and Title](#)

**Grabherr MG, Haas BJ, Yassour M, Levin JZ, Thompson DA, et al (2011) Full-length transcriptome assembly from RNA-Seq data without a reference genome. Nat Biotechnol 29: 644-652**

Pubmed: [Author and Title](#)  
CrossRef: [Author and Title](#)  
Google Scholar: [Author Only Title Only Author and Title](#)

**Ha CM, Nam HG, Fletcher JC (2007) BLADE-ON-PETIOLE1 and 2 control Arabidopsis lateral organ fate through regulation of LOB domain and adaxial-abaxial polarity genes. Plant Cell 19: 1809-1825**

Pubmed: [Author and Title](#)  
CrossRef: [Author and Title](#)  
Google Scholar: [Author Only Title Only Author and Title](#)

**Hepworth SR, Pautot VA (2015) Beyond the divide: Boundaries for patterning and stem cell regulation in plants. Front Plant Sci 9: 1052**

Pubmed: [Author and Title](#)  
CrossRef: [Author and Title](#)  
Google Scholar: [Author Only Title Only Author and Title](#)

**Hickman AB, Perez ZN, Zhou L, Musingarimi P, Ghirlando R, et al (2005) Molecular architecture of a eukaryotic DNA transposase. Nat Struct Mol Biol 12: 715-721**

Pubmed: [Author and Title](#)  
CrossRef: [Author and Title](#)  
Google Scholar: [Author Only Title Only Author and Title](#)

**Humason GL (1979) Animal Tissue Techniques, Fourth Edition. W. H. Freeman and Company, San Francisco**

Pubmed: [Author and Title](#)  
CrossRef: [Author and Title](#)  
Google Scholar: [Author Only Title Only Author and Title](#)

**Javelle M, Marco CF, Timmermans M (2011) In Situ hybridization for the precise localization of transcripts in plants. J Vis Exp 57: e3328**

Pubmed: [Author and Title](#)  
CrossRef: [Author and Title](#)  
Google Scholar: [Author Only Title Only Author and Title](#)

**Johnston R, Wang M, Sun Q, Sylvester AW, Hake S, Scanlon MJ (2014) Transcriptomic analyses indicate that maize ligule development recapitulates gene expression patterns that occur during lateral organ initiation. Plant Cell 26: 4718-4732**

Pubmed: [Author and Title](#)  
CrossRef: [Author and Title](#)  
Google Scholar: [Author Only Title Only Author and Title](#)

**Keller T, Abbott J, Moritz T, Doerner P (2006) Arabidopsis REGULATOR OF AXILLARY MERISTEMS1 controls a leaf axil stem cell niche and modulates vegetative development. Plant Cell 18: 598-611**

Pubmed: [Author and Title](#)

CrossRef: [Author and Title](#)

Google Scholar: [Author Only Title Only Author and Title](#)

**Kelley LA, Sternberg MJE (2009) Protein structure prediction on the Web: a case study using the Phyre server. Nat Protoc 4: 363-371**

Pubmed: [Author and Title](#)

CrossRef: [Author and Title](#)

Google Scholar: [Author Only Title Only Author and Title](#)

**Kenzo T, Ichie T, Watanabe Y, Hiromi T (2007) Ecological distribution of homobaric and heterobaric leaves in three species of Malaysian lowland tropical rainforest. Amer J Bot 94: 764-775**

Pubmed: [Author and Title](#)

CrossRef: [Author and Title](#)

Google Scholar: [Author Only Title Only Author and Title](#)

**Kierzkowski D, Nakayama N, Routier-Kierzkowska A-L, Weber A, Bayer E, et al (2012) Elastic domains regulate growth and organogenesis in the plant shoot apical meristem. Science 335: 1096-1099**

Pubmed: [Author and Title](#)

CrossRef: [Author and Title](#)

Google Scholar: [Author Only Title Only Author and Title](#)

**Komatsu K, Maekawa M, Ujiie S, Satake Y, Furutani I, et al (2003) LAX and SPA: Major regulators of shoot branching in rice. Proc Natl Acad Sci USA 100: 11765-11770**

Pubmed: [Author and Title](#)

CrossRef: [Author and Title](#)

Google Scholar: [Author Only Title Only Author and Title](#)

**Langdale JA (2005) The then and now of maize leaf development. Maydica 50: 459-467**

Pubmed: [Author and Title](#)

CrossRef: [Author and Title](#)

Google Scholar: [Author Only Title Only Author and Title](#)

**Langmead B, Trapnell C, Pop M, Salzberg SL (2009) Ultrafast and memory-efficient alignment of short DNA sequences to the human genome. Genome Biol 10: R25**

Pubmed: [Author and Title](#)

CrossRef: [Author and Title](#)

Google Scholar: [Author Only Title Only Author and Title](#)

**Lee D-K, Geisler M, Springer PS (2009) LATERAL ORGAN FUSION1 and LATERAL ORGAN FUSION2 function in lateral organ separation and axillary meristem formation in Arabidopsis. Development 136: 2423-2432**

Pubmed: [Author and Title](#)

CrossRef: [Author and Title](#)

Google Scholar: [Author Only Title Only Author and Title](#)

**Leegood RC (2008) Roles of the bundle sheath cells in leaves of C3 plants. J Exp Bot 59: 1663-1673**

Pubmed: [Author and Title](#)

CrossRef: [Author and Title](#)

Google Scholar: [Author Only Title Only Author and Title](#)

**Lewis MW, Hake S (2015) Keep on growing: building and patterning leaves in the grasses. Curr Opin Plant Biol 29: 80-86**

Pubmed: [Author and Title](#)

CrossRef: [Author and Title](#)

Google Scholar: [Author Only Title Only Author and Title](#)

**Lundqvist U, Franckowiak JD (2002) BGS 623. Eligulum-a, eli-a. Barley Genet Newsl 32: 124**

Pubmed: [Author and Title](#)

CrossRef: [Author and Title](#)

Google Scholar: [Author Only Title Only Author and Title](#)

**Majorek KA, Dunin-Horkawicz S, Steczkiewicz K, Muszewska A, Nowotny M, et al (2014) The RNase H-like superfamily: new members, comparative structural analysis and evolutionary classification. Nucl Acids Res 42: 4160-4179**

Pubmed: [Author and Title](#)

CrossRef: [Author and Title](#)

Google Scholar: [Author Only Title Only Author and Title](#)

**Mathan J, Bhattacharya J, Ranjan A (2016) Enhancing crop yield by optimizing plant developmental features. Development 143: 3283-3294**

Pubmed: [Author and Title](#)

CrossRef: [Author and Title](#)

Google Scholar: [Author Only Title Only Author and Title](#)

**Milne I, Stephen G, Bayer M, Cock JA, Pritchard L, et al (2013) Using Tablet for visual exploration of second-generation sequencing data. Brief Bioinform 14: 193-202**

Pubmed: [Author and Title](#)  
CrossRef: [Author and Title](#)  
Google Scholar: [Author Only Title Only Author and Title](#)

**Moon J, Candela H, Hake S (2013) The liguleless narrow mutation affects proximal-distal signaling and leaf growth. Development 140: 405-412**

Pubmed: [Author and Title](#)  
CrossRef: [Author and Title](#)  
Google Scholar: [Author Only Title Only Author and Title](#)

**Müller D, Schmitz G, Theres K (2006) Blind homologous R2R3 Myb genes control the pattern of lateral meristem initiation in Arabidopsis. Plant Cell 18: 586-597**

Pubmed: [Author and Title](#)  
CrossRef: [Author and Title](#)  
Google Scholar: [Author Only Title Only Author and Title](#)

**Nakayama N, Smith RS, Mandel T, Robinson S, Kimura S, et al (2012) Mechanical regulation of auxin-mediated growth. Curr Biol 22: 1468-1476**

Pubmed: [Author and Title](#)  
CrossRef: [Author and Title](#)  
Google Scholar: [Author Only Title Only Author and Title](#)

**Nikovics K, Blein T, Peaucelle A, Ishida T, Morin H, Aida M, Laufs P (2006) The balance between the MIR164A and CUC2 genes controls leaf margin serration in Arabidopsis. Plant Cell 18: 2929-2945**

Pubmed: [Author and Title](#)  
CrossRef: [Author and Title](#)  
Google Scholar: [Author Only Title Only Author and Title](#)

**Oikawa T, Kyojuka J (2009) Two-step regulation of LAX PANICLE1 protein accumulation in axillary meristem formation in rice. Plant Cell 21: 1095-1108**

Pubmed: [Author and Title](#)  
CrossRef: [Author and Title](#)  
Google Scholar: [Author Only Title Only Author and Title](#)

**Quevillon E, Silventoinen V, Pillai S, Harte N, Mulder N, Apweiler R, Lopez R (2005) InterProScan: protein domains identifier. Nucleic Acids Res W116-W120**

Pubmed: [Author and Title](#)  
CrossRef: [Author and Title](#)  
Google Scholar: [Author Only Title Only Author and Title](#)

**Rozen S, Skaletsky HJ (2000) Primer3 on the WWW for general users and for biologist programmers. In: Krawetz S, Misener S (eds) Bioinformatics Methods and Protocols: Methods in Molecular Biology. Humana Press, Totowa, NJ, pp 365- 386.**

Pubmed: [Author and Title](#)  
CrossRef: [Author and Title](#)  
Google Scholar: [Author Only Title Only Author and Title](#)

**Ruzin SE (1999) Plant Microtechnique and Microscopy. Oxford University Press Inc, New York**

Pubmed: [Author and Title](#)  
CrossRef: [Author and Title](#)  
Google Scholar: [Author Only Title Only Author and Title](#)

**Schmitz G, Theres K (2005) Shoot and inflorescence branching. Curr Opin Plant Biol 8: 641-654**

Pubmed: [Author and Title](#)  
CrossRef: [Author and Title](#)  
Google Scholar: [Author Only Title Only Author and Title](#)

**Sylvester AW, Cande WZ, Freeling M (1990) Division and differentiation during normal and liguleless-1 maize leaf development. Development 110: 985-1000**

Pubmed: [Author and Title](#)  
CrossRef: [Author and Title](#)  
Google Scholar: [Author Only Title Only Author and Title](#)

**Tavakol E, Okagaki R, Verderio G, Shariati VJ, Hussien A, et al (2015) The barley Uniculme4 gene encodes a BLADE-ON-PETIOLE-like protein that controls tillering and leaf patterning. Plant Physiol 168: 164-174**

Pubmed: [Author and Title](#)  
CrossRef: [Author and Title](#)  
Google Scholar: [Author Only Title Only Author and Title](#)

**The International Barley Genome Sequencing Consortium (2012) A physical, genetic and functional sequence assembly of the barley genome. Nature 491: 711-716**

Pubmed: [Author and Title](#)  
CrossRef: [Author and Title](#)  
Google Scholar: [Author Only Title Only Author and Title](#)

**Trivett CL, Evert RF (1998) Ontogeny of the vascular bundles and contiguous tissues in the barley leaf blade. Int J Plant Sci 159: 716-723**

Pubmed: [Author and Title](#)  
CrossRef: [Author and Title](#)  
Google Scholar: [Author Only](#) [Title Only](#) [Author and Title](#)

**Van Ooijen JW (2006) JoinMap® 4, Software for the calculation of genetic linkage maps in experimental populations. Kyazma B V, Wageningen, Netherlands**

Pubmed: [Author and Title](#)  
CrossRef: [Author and Title](#)  
Google Scholar: [Author Only](#) [Title Only](#) [Author and Title](#)

**Walsh J, Waters CA, Freeling M (1998) The maize gene *liguleless2* encodes a basic leucine zipper protein involved in the establishment of the leaf blade-sheath boundary. *Genes & Develop* 12: 208-218**

Pubmed: [Author and Title](#)  
CrossRef: [Author and Title](#)  
Google Scholar: [Author Only](#) [Title Only](#) [Author and Title](#)

**Wang Q, Hasson A, Rossmann S, Theres K (2016) Divide et impera boundaries shape the plant body and initiate new meristems. *New Phytologist* 209: 485–498**

Pubmed: [Author and Title](#)  
CrossRef: [Author and Title](#)  
Google Scholar: [Author Only](#) [Title Only](#) [Author and Title](#)

**Wang Y, Li J (2008) Molecular basis of plant architecture. *Ann Rev Plant Biol* 59: 253-279**

Pubmed: [Author and Title](#)  
CrossRef: [Author and Title](#)  
Google Scholar: [Author Only](#) [Title Only](#) [Author and Title](#)

**Wenzel CL, Chandler PM, Cunningham RB, Passioura JB (1997) Characterization of the leaf epidermis of barley (*Hordeum vulgare* L. 'Himalaya'). *Annals Bot* 79: 41-46**

Pubmed: [Author and Title](#)  
CrossRef: [Author and Title](#)  
Google Scholar: [Author Only](#) [Title Only](#) [Author and Title](#)

**Wu S, Zhang Y (2007) LOMETS: A local meta-threading-server for protein structure prediction. *Nucl Acids Res* 35: 3375-3382**

Pubmed: [Author and Title](#)  
CrossRef: [Author and Title](#)  
Google Scholar: [Author Only](#) [Title Only](#) [Author and Title](#)

**Yang F, Wang Q, Schmitz G, Müller D, Theres K (2012) The bHLH protein ROX acts in concert with RAX1 and LAS to modulate axillary meristem formation in *Arabidopsis*. *Plant J* 71: 61-70**

Pubmed: [Author and Title](#)  
CrossRef: [Author and Title](#)  
Google Scholar: [Author Only](#) [Title Only](#) [Author and Title](#)

**Žádníková P, Simon R (2014) How boundaries control plant development. *Curr Opin Plant Biol* 17: 116-125**

Pubmed: [Author and Title](#)  
CrossRef: [Author and Title](#)  
Google Scholar: [Author Only](#) [Title Only](#) [Author and Title](#)